Revised 13 January to include the figures.

www.sciencemag.org/cgi/content/full/science.1199784/DC1

Supporting Online Material for

Proteome Half-Life Dynamics in Living Human Cells

Eran Eden,* Naama Geva-Zatorsky, Irina Issaeva, Ariel Cohen, Erez Dekel, Tamar Danon, Lydia Cohen, Avi Mayo, Uri Alon*

*To whom correspondence should be addressed. E-mail: eraneden@gmail.com (E.E), urialon@weizmann.ac.il (U.A.)

Published 13 January 2011 on *Science* Express
DOI: 10.1126/science.1199784

This PDF file includes

Other Supporting Online Material for this manuscript includes the following:
(available at www.sciencemag.org/cgi/content/full/science.1199784/DC1)

Movie S1

Supporting Online Material

Contents

1 Material & Methods

1.1 Box S1: Summary of bleach-chase equations

(1) Protein removal rate, α, is the sum of intra-cellular degradation, α_{deg}, and the dilution rate, α_{dil}. (2) Protein levels, $P(t)$, are dictated by the balance between production rate, $\beta(t)$, and the removal rate, $\alpha(t)$ (*1-2*). Note that production and removal may also implicitly depend on mRNA and protein levels. (3) The in-vivo half-life of a protein, $T_{1/2}$, is inversely related to the removal rate. This equation holds if α is constant. Note that the effective half-life in living cells depends on both degradation and dilution. (4) The non-fluorescent protein fraction (the difference between the fluorescence of bleached and unbleached cells) decays in time according to the removal rate. This is obtained by subtracting and solving Eq. 2 for the bleached and unbleached cells, (see Methods). $P(t)$ and $P_v(t)$ are the fluorescence levels of the unbleached and bleached cells, respectively; P_0 and P_{0v} are the fluorescence levels of the unbleached and bleached at an initial time point, respectively. Thus, the slope of the non-fluorescent protein dynamics plotted on a semi-logarithmic plot is equal to the removal rate α. If the removal rate, α, varies with time, the same equation applies, with $\alpha \cdot t$ replaced by $\int_0^t \alpha(t')\ dt'$.

Box S1 – Equations (Bleach-chase)

(1) $\alpha = \alpha_{\mathrm{deg}} + \alpha_{dil}$

(2) $\frac{dP(t)}{dt} = \beta(t) - \alpha(t) \cdot P(t)$

(3) $T_{1/2} = \frac{\ln(2)}{\alpha}$

(4) $ln\big(P(t) - P_v(t)\big) = ln(P_0 - P_{0v}) - \alpha \cdot t$

1.2 Fluorescently-tagged protein clones

Clones used in this study are from the LARC library of human non-small cell lung carcinoma (H1299), in which proteins were fluorescently-tagged at their native locus under their endogenous regulation by CD-tagging, previously described in (*3-7*). Briefly, each clone contains two tags: The first, common to all clones, is a red fluorescent protein mCherry that creates a pattern, which is brighter in the nucleus and dimmer in the cytoplasm and is used for image analysis purposes. The second is a yellow fluorescent protein tag (YFP) that is fused to the protein of interest. This produces a full-length fusion protein that operates under its native regulation. The CD-tagging scheme used to generate the clones tends to preserve protein functionality and localization (*7-11*). Comparison to immunoblots indicated that 80% of the tagged proteins are accurate markers for the endogenous protein dynamics (*7*). Note, that the purpose of this study does not require the proteins to be functional but merely to be reliable reporters of the endogenous protein dynamics. Additional information regarding the LARC library is published elsewhere (*7*).

1.3 Time-lapse microscopy

Time-lapse movies were at 20x magnification. Three automated microscopes were used, based on inverted fluorescence microscopes from Leica (one DMIRE2 and two DMI6000B). All microscopes included live cell environmental incubators maintaining 37^{o}C (37-2 digital and Heating unit, PeCon,Germany, Leica #15531719), humidity and 8% CO_2 (PeCon, GmbH, Germany #0506.000-230, Leica #11521733) and automated stage movement control (Corvus, ITK, GmbH, Germany); stage was incubated to maintain constant temperature, CO_2 concentration, and humidity. Transmitted and fluorescent light paths were controlled by electronic shutters (Uniblitz, model VMM-D1, Rochester, NY); Fluorescent light sources were Short ARC Lamp HXP R 120w/45C VIS (OSRAM, Germany). Cooled 12 and 14 bit CCD cameras were used: QImaging, (RETIGA-S&V, Fast 1394, RET-SRV-F-M-12-C, Canada); CoolSNAP, (Roper Scientific HQ, photometrics); ORCA-ER (C4742-95-12ERG, and Hamamatsu photonics K.K, Japan). The following single channel filters (Chroma Technology Corp) were used: YFP (500/20 nm excitation, 515 nm dichroic splitter, and 535/30 nm emission, Chroma #41028) and mCherry Red (575/50 nm excitation, 610 nm dichroic splitter, and 640/50nm emission, Chroma #41043). Hardware was controlled by ImagePro5 Plus software (Media Cybernetics) with integrated time-lapse acquisition, stage movement, and software based auto-focus.

Cells were grown and visualized in 12-well optical glass-bottom plates (MatTek cultureware, Microwell plates-uncoated, part No. P12G-0-14-F, Lot No. TK0289) coated with 10µM fibronectin 0.1% (solution from bovine plasma, Sigma, Cat. No. F1141) diluted 1:100 in Dulbecco's Phosphate Buffered Saline, PBS (Sigma, Cat. No. D8537). For

each well, time-lapse movies were obtained at four fields of view. Each movie was taken at a time resolution of 20 minutes and was filmed for one or two days (72 and 144 time points respectively). Each time point included a transmitted light image (phase contrast), and two fluorescent channel images (red and yellow). No significant bleaching was observed (on average less than 3% over the duration of the experiment). For each protein, the population average dynamics was obtained by averaging over the profiles of ~500 individual cells.

1.4 Image analysis of time lapse movies

Custom computer vision software, *PhenoTrack*, automatically extracted quantitative measurements of protein dynamics from time-lapse movies. The main modules in the software include background normalization, cell segmentation, cell tracking and automated identification of various cellular phenotypes (e.g. mitosis and cell death). The PhenoTrack software was implemented in Matlab and C++.

1.5 Tissue culture media

Cells were grown in RPMI 1640 supplied with (+) L-Glutamine (GIBCO, cat. No. 21875) medium supplemented with 10% Fetal Calf Serum (certified fetal bovine serum, membrane filtered, Biological Industries, 04-001-1A) and 0.05% Penicillin-Streptomycin antibiotics (Biological Industries Cat. No. 03-031-1B). Cells were grown in incubators at 37^{o}C and 8% CO_2.

1.6 Stress induction under the microscope

In each experiment, the drug was diluted to the desired concentration in transparent growth medium (RPMI 1640, 0.05% Penicillin-Streptomycin antibiotics, 10% FCS, with L-Glutamine, lacking riboflavin and phenol red, Bet Haemek, Biological Industries Cat. No. 06-1100-26-1A). Normal transparent growth medium (2ml, without the drug) was replaced by the diluted drug under the microscope after bleaching the cells (2ml medium with a final concentration of 10µM for CPT, 1 µM for paclitaxel, 80 µM for cisplatin and 1ug/ml for actinomycin-D diluted from stock, see 1.7). In starvation experiments, normal medium was washed twice with transparent growth medium without serum. Then, transparent medium with the desired 0% serum concentration was added and cells were starved in these conditions for 48hrs prior to the bleaching experiment.

1.7 Drugs

Camptothecin (CPT, C9911 Sigma) and Paclitaxel (T7402, Sigma) were dissolved in DMSO (hybri-max, D2650 Sigma), giving a stock solution of 10mM. Cisplatinum (P4394 Sigma) was dissolved in DMSO giving a stock solution of 100mM. Actinomycin-D (A1410 ,Sigma) was dissolved in DMSO giving a stock solution of 1mg/ml.

1.8 Pulse-chase protocol for measuring protein half-lives

Approximately $2x10^6$ cells were plated onto 10 cm dishes and cultured for 24 hours as described above. To perform pulse-chase, cell monolayers were rinsed twice with warm sterile PBS and starved of methionine and cysteine for 1 h at 37 ^oC by incubation in 5ml of Pulse-chase medium: methionine/cysteine-free RPMI 1640 (Sigma, R-7513) supplemented with 10% dialyzed FBS (Biological Industries Beit Haemek) and 2mM L-glutamine. Following starvation, the cells were labeled for 1 hour at 37 ^oC with 4 ml of Pulse-chase medium containing 1 mCi (250 µCi/mL) of [35S]methionine/cysteine (EasyTag^{TM}Expre^{35}S^{35}S Protein Labeling Mix, #PENEG772, PerkinElmer). The radioactive medium was then removed, the cells rinsed three times with PBS, re-fed with Pulse-chase medium supplemented with 2.5 mM L-Methionine and 2.5 mM L-Cysteine Hydrochloride Hydrate (Biological Industries Beit Haemek), and incubated for the indicated times. The cells were then collected and lysed with modified RIPA buffer (50 mM Tris-HCl , pH 7.4; 150 mM NaCl; 1 mM EDTA; 1% NP-40; 0.25% Na-deoxycholate; 1 mM PMSF and 1 µg/ml of each aprotinin, leupeptin and pepstatin). Protein concentrations were determined by BCA protein assay (Thermo Scientific). The proteins of interest were recovered from 200 µg of cell lysates by immunoprecipitation using anti-GFP or protein-specific antibodies listed below. The immunoprecipitates were subjected to SDS-PAGE, and protein bands were detected by autoradiography. Parallel gels were blotted onto nitrocellulose membrane and probed with protein-specific antibodies to ensure correct identification of the protein bands of interest.

The following antibodies were used in the study:

Antibody against Myosin IIA/MYH9 (M8064) was purchased from Sigma; anti-GFP antibody (11814460001) was purchased from Roche; antibodies against p68/DDX5 (sc-32858), Trx (sc-20146), OP18/STMN1 (sc-55531), normal rabbit IgG (sc-2027) and normal mouse IgG (sc-2025) were purchased from Santa-Cruz; anti-K-α-1/Tubulin α (ab44928 and ab15246) and anti-DDX18 (ab70527) antibodies were obtained from Abcam.

For immunoprecipitation each antibody was used at amount of 9 µg. For immunoblot analysis the antibodies were diluted as following: anti-GFP 1:600, anti-MYH9 1:800, anti-DDX5 1:300, anti-Tubulin 1:150, anti-Trx 1:250, anti-DDX18 1:1000, anti-STMN1 1:200.

To determine protein half-lives, intensities of the relevant protein bands were quantified from the autoradiographs using custom Matlab software. We assumed that the levels of the radioactive labeled protein, $P(t)$, decay in time at a rate that is exponential in the removal rate, α according to the following equation:

$$\text{Eq. (5)} \quad P(t) = P_0 e^{-\alpha \cdot t} ,$$

where P_0 is protein band intensity at t = 0. The removal rate, α, is retrieved by applying a linear regression to the following equation:

$$\text{Eq. (6)} \quad \ln\big(P(t)\big) = \ln(P_0) - \alpha \cdot t.$$

1.9 Bleach chase: mathematical analysis

In this section we describe how bleach-chase works by deriving Eq. 4 in Box 1 used for removal rate measurement and then describe the experimental protocol. Assume a fluorescently tagged protein whose removal rate, α, is constant in time (similar equations can be devised for the more general case where α changes in time). By exposing the cells to a brief pulse of light one can bleach a fraction of the proteins inside the cells, effectively transforming them from fluorescently tagged into non-fluorescent. We can therefore think of the total protein, P, as the sum of two cohorts of proteins, one visible to fluorescent microscopy, P_v, and another which is invisible, $\tilde{P}$:

$$Eq.(7) \quad P(t) = P_v(t) + \tilde{P}(t).$$

The invisible protein $\tilde{P}$ is produced only during the pulse, after which it starts to degrade according to the following equation:

$$Eq.(8) \quad \frac{d\tilde{P}(t)}{dt} = -\alpha * \tilde{P}(t).$$

Hence, measurement of how $\tilde{P}$ changes in time would enable the retrieval of the removal rate. But, since $\tilde{P}$ is invisible it cannot be measured directly. The solution is to retrieve it indirectly by measuring P and P_v and applying Eq. 7 and 8:

$$Eq.(9) \quad \frac{d(P(t) - P_v(t))}{dt} = -\alpha * (P(t) - P_v(t)).$$

The solution to this equation means that the difference between the bleached and non-bleached experiment decays exponentially in time at a rate that depends solely on the removal rate of the protein under study:

$$Eq.(10) \quad (P(t) - P_v(t)) = (P_0(t) - P_{v0}(t))\, e^{-\alpha t}.$$

and hence we derive Eq. 4 in Box 1:

$$ln\,(P(t) - P_v(t)) = ln(P_0(t) - P_{v0}(t)) - \alpha \cdot t.$$

Hence one can retrieve α by measuring $P(t)$ and $P_v(t)$ at multiple time points and applying a linear regression. The slope of the fit is the removal rate α. One can relax the assumption that the removal rate is constant in time by applying $\alpha(t)$ instead of α in Eq. 9 and solving the new set of equations.

1.10 Bleach-chase protocol

Protein fluorescence was measured with and without the drug in 12 well plates using multiple fields of view under time lapse microscopy as described in previous sections. However, in bleach-chase two concurrent measurements are done: without and with the bleaching. The latter was done using a pulse of light given one round prior to drug addition. In the rest of the time-lapse normal exposure times are used that are sufficient to detect the protein under study. We tested a range of pulse durations (0.5 - 8 minutes) using a mercury fluorescent lamp (120W) resulting in different fractions of the protein fluorescence bleaching (10% - 60% drop). Note that the measured removal rates were roughly insensitive to the degree of bleaching (CV < 0.2).

Our dynamic proteomics experiments generate temporal traces of hundreds of individual cells. To compute population averages we smooth the temporal dynamics of each individual cell using a median sliding window (window size = 3), and average the protein levels over all cells at each time point (illustrated in Fig. 1A). To obtain robust measurements of the removal rate, α, we perform a linear regression using Eq. 4 in Box 1. As linear fits may be sensitive to outliers, we perform the following quality assurance scheme: First, we estimate α using a non-linear fit based on Eq. 10. If it deviated from the linear fit by more than a factor of two and more than three hours the measurement was discarded. Second, we estimated the confidence intervals of the fit by computing the maximal and minimal removal rates whose MSE is 5% larger than the optimal fit. If they deviated from the optimal fit by more than a factor of three, the experiment was discarded. We performed at least three day-to-day repetitions for each protein, and computed α by averaging the results of all the experiments.

Note, that bleach-chase is different from fluorescence recovery after photo-bleaching (FRAP), which is used to measure lateral diffusion (*12-13*). It is similar in principle to light activation of photoactivatable fluorescent proteins (*14-15*), but unlike these, can be readily applied to existing libraries of non-activatable fluorophore tagged proteins (*7, 10, 16*).

1.11 Measuring the dilution rate

To obtain the dilution rate, we tracked ~10,000 individual cells and recorded the average time between two mitosis events. The average cell-cycle duration was $T_{cc} = 22.5 \pm 2.6$ hours, resulting in an average dilution rate of α_{dil} = 0.031 1/hours (because $\alpha_{dil} = \ln(2)\,/T_{cc}$). We note that the dilution rate under normal conditions is largely independent of the duration it is measured as long as cells have not reached confluency. We observed similar dilution rates when tracking the cells for 24, 48, 72 and 96 hours. A previous study that measured the growth rate in the same cells using an independent experimental method (FACS) reached similar results for the cell-cycle duration (*11*). Degradation rates were obtained by subtracting the dilution rate from the removal rate (according to Eq. 1 in Box S1).

1.12 Derivation of reduced dilution model

In this section we derive Eq. 5 in Fig. 3C, that captures the expected change in half-life, $T^*_{1/2}$, as a function of the half-life prior to the change, $T_{1/2}$, the cell cycle duration, T_{cc}, and the fold change in growth rate, k. By applying Eq. 1-3 in Box S1, it follows that:

$$Eq.(11) \quad T_{1/2} = \frac{\ln(2)}{\alpha_{\mathrm{deg}} + \alpha_{\mathrm{dil}}},$$

$$Eq.(12) \quad T^*_{1/2} = \frac{\ln(2)}{\alpha_{\mathrm{deg}} + \mathrm{k} \cdot \alpha_{\mathrm{dil}}},$$

$$Eq.(13) \quad T_{CC} = \frac{\ln(2)}{\alpha_{\mathrm{dil}}}.$$

Substituting Eq. 11 and 13 into Eq. 12 yields:

$$T^*_{1/2} = \frac{\ln(2)}{\alpha_{\mathrm{deg}} + \alpha_{\mathrm{dil}} + (\mathrm{k}-1) \cdot \alpha_{\mathrm{dil}}} = \frac{\ln(2)}{\frac{\ln(2)}{T_{1/2}} + (k-1)\frac{\ln(2)}{T_{CC}}},$$

and hence we derive Eq. 5 in Fig. 3C:

$$T^*_{1/2} = \frac{T_{1/2}}{1 + (k-1)\frac{T_{1/2}}{T_{cc}}}$$

1.13 Translation inhibition protocol for measuring protein half-lives

We sought to compare our bleach-chase and pulse-chase half-life measurements to translation inhibition based measurements (for details see Section 5.2 in the Supporting text). This section describes the experimental protocol of the latter. Cyclohexamide (CHX, C4859 – Ready-made solution, 100mg/ml in DMSO, Sigma) was diluted in transparent growth medium to 10µM. Normal transparent growth medium (2ml, without CHX) was replaced by the 2ml diluted CHX under the microscope after at least one round without the CHX. The dynamic profiles of the proteins were then measured for 20 hours (20 minutes resolution) using time-lapse microscopy as described in previous sections.

Measurements were done on 11 proteins (DDX5, CKS2, ENO1, JAGN1, DNCH1, RPS3, LMNA, MAP2K2, NCBP2, PSMB4 and RPL22) with at least two replicates. Assuming

that the translation inhibitor CHX completely halts protein production would result in a time dependent exponential decay to zero according to Eq. 10. However, in practice about half of the tested protein showed dynamics that did not fit an exponential decay to zero (e.g. CKS2) and one protein, ENO1, showed an increase in response to CHX (Figure S1). This indicates that in the present human cells CHX does not halt translation but only reduces it (increasing CHX dosage by 10 fold gave similar protein profiles). Hence, retrieving removal rates from the present measurements requires a model that allows for both production and removal. We tested several models but found that the estimated removal rate can change considerably (factor of 10) according to the arbitrary choice of model. Overall, we were unable to obtain reliable removal rates in the present human cells using a CHX based approach.

1.14 GO Enrichment analysis

GO enrichment analysis was used to identify groups of genes with similar half-lives that also share similar function or localization. This was done by ranking the proteins according to their half-lives and seeking functions or localizations that are enriched at either end of the list using the mHG procedure (*17-18*). The mHG P-value is similar to the hyper geometric P-value but it does not require a predetermined arbitrary cutoff for determining the target and the background sets.

2 Supplementary Movie captions

Movie S1. Bleaching and recovery of the RPS3A protein in individual living human cells.

3 Supplementary Figure captions

Figure S1. Protein profiles in response to the translation inhibitor CHX. The dynamic profiles of 11 protein were measured in response to 10μM of the translation inhibitor CHX. Colored lines and black line indicate the response of individual cells and the average response respectively. All values were normalized to the average level at t = 0 hours. Following the addition of CHX it is expected that protein production will halt and that the protein levels will gradually decay to zero in a rate that is exponential in the removal rate. However, in practice we observed one protein, ENO1, that increased and about half of the tested proteins showed dynamics that did not fit an exponential decay to zero (e.g. CKS2). This suggests that in the present cells translation inhibition was incomplete. Increasing the dosage of CHX did not eliminate this effect.

Figure S2. Examples of autoradiographs pulse-chase results for MYH9 and DDX5. The H1299 cells expressing the YFP tagged protein of interest were pulse-labeled with [35S] methionine/cysteine followed by cold chase as described in the Methods. At the times indicated, the cells were collected and whole cell lysates were prepared. The proteins of interest were recovered from 200 μg of cell lysates by immunoprecipitation (IP). Anti-GFP antibody was used to precipitate the YFP tagged proteins; protein-specific Abs were used to precipitate both the YFP tagged and the wild type forms of the proteins; non-specific rabbit or mouse IgG was used as a negative control. The immunoprecipitated proteins were resolved on SDS-PAGE and visualized by autoradiography (the left panels). Parallel gels were blotted onto nitrocellulose membrane and probed with the indicated antibodies (the right panels) to ensure correct identification of the protein bands of interest. About 20-40 μg of cell lysates (10-20% of the amount used for IP) were loaded on the gels as positive controls (Input). Each experiment was done with at least two biological replicates. To determine protein removal rates, intensities of the relevant protein bands were quantified from the autoradiographs using a custom Matlab software. Levels of the radioactive labeled protein were plotted on a semi-logarithmic scale. The slope of the linear fit is the removal rate.

Figure S3. Removal rate measurements are invariant to the amount of bleaching. The CPT response of RPS3A was measured without bleaching (blue dots) and after two and four minutes of bleaching (red and green dots respectively). The convergence rate in both cases yielded similar removal rates (0.08 ± 0.01 and 0.09 ± 0.01 1 / hour).

Figure S4. The observed differential increase in half-lives is statistically significant. We hypothesized that the longer the half-life of a protein, the larger its increase due to growth arrest. To assess the statistical significance of this assertion we performed the following Monte-carlo shuffling test. First, we computed the deviation (absolute sum of differences) of the measured half-lives after drug from the predicted half-lives due to growth arrest. Then, we shuffled the *changes* in half-lives ($T_{1/2}$ after drug) – ($T_{1/2}$ before drug), and added each of them to the pre-drug half-lives of a randomly selected protein. The null distribution generated by computing the absolute sum of differences over multiple shuffle rounds is shown, yielding a $P < 10^{-4}$.

Figure S5. Protein half-lives at t=0-24 and t=24-48 hours after addition remain roughly constant or increase. (A, B) The half-lives of 10 proteins at t = 0 – 24 and t = 24 - 48 hours after drug addition are compared. Most half-lives remained approximately constant or slightly increased. CALM2 and K-α-1 showed a substantial increase in their half-lives. Blue line indicates the predicted increase due to growth arrest.

Figure S6. A few proteins increased their removal in response to the drug CPT. We sought to identify proteins whose half-lives after the drug CPT deviated from the growth arrest model (depicted in Fig. 2A). To this end we computed the $\log_2$ ratio between the expected and observed post-drug half-lives. We subtracted or added the measurement error from the observed half-life of each protein so as to minimize this ratio. This correction procedure yields conservative estimations of the ratio (lower bound). The three proteins that showed the most significant deviation, CD44, DDX18 and RPS3A, increased their removal rates in response to the drug, suggesting protein specific removal regulation.

Figure S7. A simulation comparing 'average protein concentration' versus 'average protein levels' dynamics. (A) Top to bottom panel show: (i) Number of cells as a function of time (in units of cell-cycle) starting with one cell and assuming cell-cycle length variability of 25% across individual cells; (ii) Protein levels of individual cells (in arbitrary units); (iii) Volume of individual cells; (iv) Total protein in the population; (v) Total volume of the population; (vi) 'Average protein concentration' (i.e. total protein divided by the total volume of the population) and (vii) 'Average protein levels' (i.e. total protein divided by the number of cells). Following the measurements of (*19*) we use a cell volume that increases exponentially in the cell cycle phase, and protein levels that are proportional to the volume per individual cell. Notice that following a few synchronized cells, results in fluctuating amounts of average protein level, yet robust levels of protein concentration. (B-C) Initial number of cells of non-synchronized cells is 10 and 100 respectively. It can be seen that the average protein levels is more robust the larger the population. Notice that the average protein levels are larger than one reflecting the amount of protein half-way through the cell-cycle.

Figure S8. Expected increase in half-lives due to degradation inhibition does not account for the observed response to the drug CPT. Reducing degradation is expected to increase protein half-lives such that the longer the half-life, the smaller the increase. Protein half-lives before and after CPT addition are shown. The curved lines illustrate the predicted increase in half-lives due to reduced degradation. They are obtained by setting k_1 to 100%, 50%, 20% and 10% (reflecting the fold reduction in degradation) and applying Eq. 3 in Fig. 2. This pattern does not account for observed half-life increase in response to the drug.

4 Supplementary Tables

Table S1. **Protein half-life measurements of bleach-chase and pulse-chase agree.** We measured the half-lives of six proteins using bleach-chase (no. of day-to-day repeats ≥ 3) and radioactive pulse-chase (no. of day-to-day repeats ≥ 2) (for details see Methods). The difference between the two methods was assessed using the following formula $(|\boldsymbol{T}_{\mathbf{1/2}}^{\boldsymbol{bleach-chase}} - \boldsymbol{T}_{\mathbf{1/2}}^{\boldsymbol{pulse-chase}}|)/(\boldsymbol{T}_{\mathbf{1/2}}^{\boldsymbol{bleach-chase}} + \boldsymbol{T}_{\mathbf{1/2}}^{\boldsymbol{pulse-chase}})$ / **2**. Average difference was 10%.

Gene Symbol	Bleach-chase $T_{1/2}$ (hours)	Pulse-chase $T_{1/2}$ (hours)	Difference (%)
STMN1	3.9 ± 0.6	3.7 ± 0.5	5%
MYH9	6.4 ± 0.6	5.7 ± 0.6	12%
RPS3A	6.7 ± 0.9	6.6 ± 0.3	1%
TXN1	8.6 ± 1.6	9.8 ± 0.5	13%
DDX5	8.7 ± 1.0	9.6 ± 0.4	10%
K-α-1	15.3 ± 2.4	18.9 ± 4.5	21%
DDX18	22.5 ± 1.4	>22.5	NA

Table S2. **Protein half-lives of YFP-tagged and untagged proteins are similar.** We measured the half-lives of YFP-tagged and their corresponding native untagged proteins using pulse-chase coupled with protein specific antibodies (as described in the Methods). In 5 out of 6 cases we find that the YFP-tagged and its corresponding native protein showed similar half-lives (average difference of 14%).

Gene Symbol	Untagged protein $T_{1/2}$ (hours)	YFP-tagged protein $T_{1/2}$ (hours)	Difference (%)
MYH9	5.2 ± 0.3	5.7 ± 0.6	9%
DDX5	8.2 ± 0.9	9.6 ± 0.4	16%
TXN1	13.0 ± 0.7	9.8 ± 0.51	28%
K-α-1	19.7 ± 3.8	18.9 ± 4.5	4%
DDX18	>22.5	>22.5	NA
STMN1*	7.8 ± 0.4	3.7 ± 0.5	71%

* immunoblots showed a missing 17KD in the YFP tagged protein possibly due to a truncation caused by the tagging. This may account for the observed discrepancy between the half-life of tagged and untagged STMN1.

Table S3. **A summary of previous studies that compared the half-lives and dynamics of tagged and untagged proteins.**

Ref.	Cell type	Comparison results
(*20*)	S. cerevisiae	Both Hmg2p-GFP and wild-type Hmg2p were degraded at similar Rates
(*21*)	HeLa & HEK293	IkBa fused to GFP showed the same half-life as the wild-type protein
(*22*)	HeLa	IkBa fused to a red fluorescence protein showed the same half-life as the wild-type protein
(*23*)	HeLa	HPV-18 E2 fused to GFP and native proteins present the same half-lives
(*24*)	S. cerevisiae	Tagging did not alter the ubiquitine/proteasome degradation of Clb2 and Sic1 in TAP tagged protein
(*25*)	S. cerevisiae	A half-life comparison of 24 different TAP tagged and untagged proteins suggested that the effect of the tagging on protein stability was secondary to other sources of error in the experiments.
(5, 7-8)		These studies found good agreement between the dynamics of endogenously tagged and untagged proteins in different cell types.

Table S4. **Protein half-lives under normal growth condition as measured by bleach-chase**

Gene symbol	Description	$T_{1/2}$ under normal growth (hours)
ANXA2	annexin A2 isoform 1	6.1 ± 0.5
BAG1	BCL2-associated athanogene.	5.3 ± 1.6
C1QBP	complement component 1, q subcomponent binding	5.7 ± 2.5
CALM2	calmodulin 2	6.7 ± 1.1
CD44	CD44 antigen isoform 1 precursor	20.8 ± 1.9
CIRBP	cold inducible RNA binding protein	6.9 ± 2.1
CKS2	CDC28 protein kinase 2	2.6 ± 1.6
COPS6	COP9 signalosome subunit 6	5.4 ± 1.0
COTL1	coactosin-like 1	8.4 ± 1.4
COX7C	cytochrome c oxidase subunit VIIc precursor	22.5 ± 5.1
DDX18	DEAD (Asp-Glu-Ala-Asp) box polypeptide 18	20.3 ± 1.4
DDX46	DEAD (Asp-Glu-Ala-Asp) box polypeptide 46	7.9 ± 2.2
DDX5	DEAD (Asp-Glu-Ala-Asp) box polypeptide 5	8.7 ± 1.0
DNMT1	DNA (cytosine-5-)-methyltransferase 1	6.9 ± 2.0
DYNC1H1	dynein, cytoplasmic, heavy polypeptide 1	13.8 ± 4.3
EEF1A1	eukaryotic translation elongation factor 1 alpha	9.9 ± 0.6
EEF1E1	eukaryotic translation elongation factor 1	2.7 ± 0.7
EEF2	eukaryotic translation elongation factor 2	8.8 ± 0.7
EIF2S2	eukaryotic translation initiation factor 2 beta	8.3 ± 1.5
EIF2S3	eukaryotic translation initiation factor 2,	10.5 ± 2.5
EIF4A1	eukaryotic translation initiation factor 4A	7.3 ± 1.2
EIF4E	eukaryotic translation initiation factor 4E	11.7 ± 0.9
EIF4EBP1	eukaryotic translation initiation factor 4E	8.5 ± 2.3
EIF4G3	eukaryotic translation initiation factor 4	8.8 ± 1.1
EIF4H	eukaryotic translation initiation factor 4H	16.3 ± 6.2
EIF5B	eukaryotic translation initiation factor 5B	8.9 ± 2.8
ENO1	enolase 1	8.0 ± 3.5
FAU	ubiquitin-like protein fubi and ribosomal	12.2 ± 1.2
FSCN1	fascin 1	5.8 ± 0.2
GAPDH	glyceraldehyde-3-phosphate dehydrogenase	0.8 ± 0.8
H2AFV	H2A histone family, member V isoform 2	13.9 ± 1.8
HAT1	histone acetyltransferase 1 isoform a	8.5 ± 1.2
HDAC2	histone deacetylase 2	4.5 ± 2.4
HMGA1	high mobility group AT-hook 1 isoform a	11.1 ± 1.5
HSP90AA1	heat shock protein 90kDa alpha (cytosolic),	4.2 ± 1.8
HSP90AB1	heat shock 90kDa protein 1, beta	8.8 ± 2.4
HSPA4L	heat shock 70kDa protein 4-like	10.6 ± 2.7

HSPH1	heat shock 105kD	16.5	±	4.2
ILF2	interleukin enhancer binding factor 2	16.5	±	3.5
K-α-1	tubulin, alpha 1b	15.3	±	2.4
LMNA	lamin A/C isoform 2	12.8	±	2.2
MYH9	myosin, heavy polypeptide 9, non-muscle	6.4	±	0.6
NASP	nuclear autoantigenic sperm protein isoform 1	16.3	±	2.3
NCL	nucleolin	13.9	±	2.8
NDUFAF2	NADH dehydrogenase (ubiquinone) 1 alpha	6.6	±	1.4
NDUFB11	NADH dehydrogenase (ubiquinone) 1 beta	10.8	±	1.2
NPM1	nucleophosmin 1 isoform 1	5.2	±	0.1
PLEC1	plectin 1 isoform 6	11.7	±	4.6
POLR2F	DNA directed RNA polymerase II polypeptide F	5.4	±	1.8
POLR2L	DNA directed RNA polymerase II polypeptide L	10.5	±	2.6
POLR3GL	polymerase (RNA) III (DNA directed) polypeptide	3.5	±	0.0
POMP	proteasome maturation protein	7.0	±	2.9
PRDX5	peroxiredoxin 5 precursor, isoform a	9.4	±	2.6
PSMA1	proteasome alpha 1 subunit isoform 2	8.8	±	3.1
PSMA3	proteasome alpha 3 subunit isoform 1	4.0	±	4.4
PSMA7	proteasome alpha 7 subunit	9.0	±	2.6
PSMB1	proteasome beta 1 subunit	6.7	±	0.1
PSMB4	proteasome beta 4 subunit	7.3	±	0.8
PSMB6	proteasome beta 6 subunit	8.5	±	4.7
PSMB7	proteasome beta 7 subunit proprotein	5.1	±	0.7
PSMC1	proteasome 26S ATPase subunit 1	5.2	±	1.5
PSMC4	proteasome 26S ATPase subunit 4 isoform 1	4.4	±	1.2
PSMD12	proteasome 26S non-ATPase subunit 12 isoform 1	4.0	±	2.0
RFC1	replication factor C large subunit	9.3	±	1.5
RPA2	replication protein A2, 32kDa	11.2	±	2.0
RPL11	ribosomal protein L11	14.9	±	2.3
RPL18	ribosomal protein L18	9.2	±	2.0
RPL22	ribosomal protein L22 proprotein	11.1	±	2.8
RPL27	ribosomal protein L27	15.4	±	3.1
RPL27A	ribosomal protein L27a	4.2	±	1.9
RPL29	ribosomal protein L29	4.8	±	1.8
RPL30	ribosomal protein L30	6.1	±	0.6
RPL39	ribosomal protein L39	3.4	±	0.5
RPL6	ribosomal protein L6	9.3	±	1.6
RPS19BP1	S19 binding protein	21.8	±	0.9
RPS2	ribosomal protein S2	19.7	±	3.5
RPS3	ribosomal protein S3	5.5	±	2.4
RPS3A	ribosomal protein S3a	6.7	±	1.0
RPS6	ribosomal protein S6	14.4	±	3.5
RPS7	ribosomal protein S7	4.3	±	1.3

RPS8	ribosomal protein S8	3.0	±	0.2
SLBP	histone stem-loop binding protein	8.2	±	1.1
SSBP1	single-stranded DNA binding protein 1	6.9	±	0.3
STMN1	stathmin 1	3.9	±	0.6
TARS	threonyl-tRNA synthetase	6.6	±	1.1
TBCA	tubulin-specific chaperone a	2.4	±	0.0
TFAM	transcription factor A, mitochondrial	16.3	±	3.7
TIMM23	translocase of inner mitochondrial membrane 23	7.8	±	1.5
TOMM70A	translocase of outer mitochondrial membrane 70	6.5	±	1.3
TUBA1C	tubulin alpha 6	8.2	±	8.6
TUBB2C	tubulin, beta, 2	5.1	±	0.5
TXN	thioredoxin	6.9	±	1.6
TXNRD1	thioredoxin reductase 1	6.6	±	0.2
UBA52	ubiquitin and ribosomal protein L40 precursor	10.8	±	2.4
UBE2K	ubiquitin-conjugating enzyme E2-25K isoform 1	6.3	±	0.8
UBE2N	ubiquitin-conjugating enzyme E2N	14.9	±	2.3
UBE2V2	ubiquitin-conjugating enzyme E2 variant 2	5.6	±	1.4
VCL	vinculin isoform meta-VCL	11.7	±	2.1
VIL2	villin 2	11.1	±	3.1
VIM	vimentin	4.9	±	0.1

Table S5. **Protein half-lives before and after CPT addition**

Gene symbol	T1/2 under normal growth (hours)	T1/2 after CPT addition (hours)
BAG1	5.3 ± 1.6	9.5 ± 1.5
CKS2	2.6 ± 1.6	1.3 ± 0.8
DDX5	8.7 ± 1.0	12.9 ± 3.5
DYNC1H1	13.8 ± 4.3	25.9 ± 3.5
EEF2	8.8 ± 0.7	7.9 ± 1.8
ENO1	8.0 ± 3.5	26.3 ± 7.3
GAPDH	0.8 ± 0.2	1.7 ± 0.4
LMNA	12.8 ± 2.2	31.0 ± 7.0
MYH9	6.4 ± 0.6	13.2 ± 3.6
PSMB4	7.3 ± 0.8	10.9 ± 3.6
RPS3A	6.7 ± 1.0	3.2 ± 0.6
STMN1	3.9 ± 0.6	11.3 ± 2.0
FSCN1	5.8 ± 0.2	13.1 ± 4.0
H2AFV	13.9 ± 1.8	>48 ± NA
K- α -1	15.3 ± 2.4	30.9 ± 8.1
NASP	16.3 ± 2.3	>48 ± NA
RPS3	5.5 ± 2.4	4.2 ± 1.6
RPS7	4.3 ± 1.3	4.4 ± 2.1
VCL	11.7 ± 2.1	38.5 ± 8.0
VIL2	11.1 ± 3.1	23.0 ± 4.0
VIM	4.9 ± 0.1	16.1 ± 3.9
CALM2	6.7 ± 1.1	11.5 ± 2.9
CD44	20.8 ± 1.9	16.0 ± 5.0
COTL1	8.4 ± 1.4	9.5 ± 1.0
DDX18	20.3 ± 1.4	22.5 ± 4.2
ILF2	16.5 ± 3.5	34.1 ± 8.1
RFC1	9.3 ± 1.5	18.4 ± 4.6
RPA2	11.2 ± 2.0	21.9 ± 4.1
RPL22	11.1 ± 2.8	14.9 ± 2.3
TARS	6.6 ± 1.1	11.6 ± 1.4
VPS26A	10.6 ± 2.3	15.3 ± 6.9
RPS6	14.4 ± 3.5	21.3 ± 7.8

Table S6. **Protein half-lives after addition of the drug paclitaxel**

Gene symbol	T1/2 after paclitaxel addition (hours)		
BAG1	11.5	±	2.6
CKS2	3.5	±	1.4
DDX5	16.4	±	1.6
H2AFV	39.2	±	5.7
LMNA	>48	±	NA
NASP	>48	±	NA
RPS7	2.5	±	0.9
VIL2	>48	±	NA

Table S7. **Protein half-lives during serum starvation**

Gene symbol	T1/2 after starvation (hours)		
BAG1	12.7	±	0.3
CKS2	5.0	±	1.2
DDX5	14.9	±	5.0
H2AFV	>48	±	NA
LMNA	25.5	±	3.0
NASP	33.0	±	3.5
RPS7	4.6	±	0.3
VIL2	31.3	±	5.0

Table S8. **Protein half-lives after addition of the drug cisplatin**

Gene symbol	T1/2 after cisplatin addition (hours)		
BAG1	5.6	±	0.9
CKS2	0.9	±	1.3
DDX5	6.1	±	1.4
H2AFV	20.5	±	1.6
LMNA	8.0	±	2.1
NASP	15.8	±	2.3
RPS7	2.7	±	0.2
VIL2	14.5	±	6.1

Table S9. **Protein half-lives after addition transcription inhibitor actinomycin-D**

Gene symbol	$T_{1/2}$ after actinomycin-D addition		
BAG1	14.9	±	12.0
CKS2	3.2	±	1.3
DDX5	9.9	±	1.9
H2AFV	34.6	±	15.1
NASP	36.2	±	11.8

5 Supporting Text

5.1 Measuring protein half-lives based on total protein divided by the number of cells leads to similar results as protein concentration based measurements

Protein dynamics is often modeled in terms of '*protein concentration*'. However, experimental methods, such as protein fluorescence assays, often do not allow direct measurements of concentration, but rather monitor the '*total protein*' levels in an individual cell or population. Here, we show that averaging the total protein levels over a sufficiently large population of unsynchronized cells leads to half-life measurements that are similar to those obtained in protein concentration based measurements.

We begin with a few definitions. The total protein level, P_t, over a population of N cells is the sum of individual cell protein levels, P_i:

$$Eq.1 \quad P_t = \sum_{i=1}^{N} P_i = N \cdot \bar{P}$$

where $\bar{P}$ is the average protein level. The total volume of a cell population, V_t, is the sum of individual cell volumes, V_i:

$$Eq.2 \quad V_t = \sum_{i=1}^{N} V_i = N \cdot \bar{V}$$

where $\bar{V}$ is the average cell volume. When measuring protein dynamics one typically monitors either the average protein concentration, $P_c = \frac{P_t}{V_t}$, or average protein levels, $\bar{P} = \frac{P_t}{N}$. The dynamics of protein concentration, P_c, is due to protein production, β_c (units of concentration per time unit), and removal, α_c (units of 1 / time) as captured by the following equation (*1-2*):

$$Eq.3 \quad \frac{dP_c}{dt} = \beta_c - \alpha_c \cdot P_c$$

The dynamics of $\bar{P}$ on a large population of unsyncronized cells is approximated by the following equation:

$$Eq.4 \quad \frac{d\bar{P}}{dt} = \bar{\beta} - \bar{\alpha} \cdot \bar{P} \,,$$

where $\bar{\beta}$ is the average protein production (units of protein per time) and $\bar{\alpha}$ is the average removal rate (units of 1 / time). Note that the production rates β_c and $\bar{\beta}$ are:

$$Eq.5 \quad \beta_c = \frac{\sum_{i=1}^{N} \beta_i}{V_t}$$

$$Eq.6 \quad \bar{\beta} = \frac{\sum_{i=1}^{N} \beta_i}{N}$$

where β_i is the total protein production in a single cell (units of protein per time). Note, that when the removal rates, α_c, and $\bar{\alpha}$ are constant, the estimated half-lives are equal to $\frac{ln(2)}{\alpha_c}$ and $\frac{ln(2)}{\bar{\alpha}}$ respectively (*2*).

Our goal is to show that when P_c and P_t are measured on a large number of unsynchronized cells (for practical purposes N > 100 is sufficient, see simulation in Figure S7) then $\alpha_c = \bar{\alpha}$. Assuming steady state over a large population of cells, Eq. 3 and Eq. 4 yield:

$$Eq.6 \quad P_c = \frac{\beta_c}{\alpha_c}$$

$$Eq.7 \quad \bar{P} = \frac{\bar{\beta}}{\bar{\alpha}}$$

The ratio between α_c and $\bar{\alpha}$ is therefore:

$$\frac{\alpha_c}{\bar{\alpha}} = \frac{\frac{\beta_c}{P_c}}{\frac{\bar{\beta}}{\bar{P}}} = \frac{\frac{\sum_{i=1}^{N} \beta_i}{V_t}}{\frac{\sum_{i=1}^{N} \beta_i}{N}} \cdot \frac{\bar{P}}{P_c} = \frac{N\bar{P}}{V_t P_c} = \frac{\frac{NP_t}{N}}{\frac{V_t P_t}{V_t}} = 1$$

This idea is summarized in the simulation shown in Figure S7.

5.2 Comparison of bleach-chase and translation inhibition

We sought to compare the protein removal rates obtained using bleach-chase to those obtained using a translation inhibition protocol (*25*). In the latter approach, protein levels are assayed at different times after the addition of the translation inhibitor Cyclohexamide (CHX). It is expected that protein production will halt, and that protein levels will gradually decay to zero. The rate of exponential decay provides a measure of the removal rate. We added the inhibitor CHX, at different concentrations and measured the levels of 11 proteins with the dynamic proteomics assay (see Methods). The results did not lend themselves to accurate estimates of the removal rates. One protein, ENO1, increased its level rather than decreased. About half of the tested proteins showed dynamics that did not fit an exponential decay to zero but rather approached a non-zero baseline, suggesting that translation inhibition was incomplete (increasing the dosage of CHX did not eliminate this effect) (Figure S1).

CHX-based measurements are known to work well for measuring the half-lives of short lived proteins (i.e. minutes to a few hours). Medium and long lived proteins require using CHX for many hours, which significantly alters the cell's biology. Since, many of the tested proteins had half-lives of more than a few hours (as measured using both pulse-chase and bleach-chase) we applied CHX for about 16h. We found that during this time the present cells stopped dividing and some underwent cell-death (~10%). This perturbation may explain, at least in part, why the CHX protocol did not yield accurate half-lives on many of the tested proteins in the present cells. It highlights the importance of non-perturbative methods for assaying removal rates.

5.3 The half-life increase due to drug addition persists for more than two cell-cycle durations

We asked whether the global increase in half-lives persists for more than one cell cycle duration. This is important because cells may require more than one cell-cycle duration in order to sense changes in their protein levels and compensate for them. To test this, we performed additional experiments and measured the half-lives of 10 proteins (CKS2, RPLA22, K-α-1, RPA2, DDX18, VIL2, CALM2, VCL, H2AFV and LMNA) for 48 hours after CPT addition at 20 minutes resolution (no. of repeats ≥ 3). Our aim was to test whether the half-life differential increase observed in the first 24 hours after drug addition persists for a longer duration (24h – 48h). In the proteins that degrade slowly, such a comparison can be done by bleaching the cells at t = 0h and then monitoring the decay of the non-fluorescent for 48 hours. However, in rapidly degrading proteins this approach is inadequate because the non-fluorescent protein disappears within a few hours. To overcome this, we applied bleach-chase at two time points: t = 0h and t = 24h hours after drug addition and traced the decay. We find that the half-lives of most proteins remained roughly constant during the first 48 hours, whereas a few proteins showed a continued increase in their half-lives (e.g. CALM2 showed a half-life of 6.7 ± 1.1 (before drug addition), 11.5 ± 2.9 (0 - 24h after drug addition) and >48h (24 – 48 after drug addition) (Figure S5). These results suggest that the half-life effect persists for the duration of at least two cell-cycles, during which the decrease in dilution is not compensated by means of increased degradation.

5.4 A decrease in intra-cellular degradation is expected to induce a global increase in half-lives in which long-lived proteins are least affected

We showed that the observed global increase of protein half-lives due to different stresses can be quantitatively captured by a decrease in growth arrest (see Fig. 3C). In this section we explore an alternative model that assumes the increase in half-lives is due to a global down-regulation of degradation (e.g. inhibition of ubiquitin-proteasome mediated proteolysis) (see Eq. 3 in Fig. 3B). Our goal is to derive this equation and show

that it does not account for the differential increase of half-life for long-lived proteins. On the contrary, long-lived proteins are expected to be the least affected.

Global inactivation of the degradation machinery (due to down regulation of one of the essential components) can be captured by to the following equation:

$$Eq.(S1) \qquad \alpha = k \cdot \alpha_{\mathrm{deg}} + \alpha_{dil},$$

where $0 \leq k \leq 1$ defines the degree of reduction in intra-cellular degradation (0 being complete inactivation and 1 no inactivation). The post-stress protein half-life, $T^*_{1/2}$, can be estimated using the half-life prior to the stress , $T_{1/2}$, and the average cell cycle time, T_{cc}. Using Eq. 1 and 3 in Box 1 and Eq. S1 one can derive the following relations:

$$Eq.(S2) \quad T_{1/2} = \frac{\ln(2)}{\alpha_{\mathrm{deg}} + \alpha_{\mathrm{dil}}},$$

$$Eq.(S3) \quad T^*_{1/2} = \frac{\ln(2)}{\mathrm{k} \cdot \alpha_{\mathrm{deg}} + \alpha_{\mathrm{dil}}},$$

$$Eq.(S4) \quad T_{CC} = \frac{\ln(2)}{\alpha_{\mathrm{dil}}}.$$

Applying Eq. S2 and S4 to S3 gives:

$$T^*_{1/2} = \frac{\ln(2)}{\mathrm{k}(\alpha_{\mathrm{deg}} + \alpha_{\mathrm{dil}}) + (1-\mathrm{k})\alpha_{\mathrm{dil}}} = \frac{\ln(2)}{k\frac{\ln(2)}{T_{1/2}} + (1-k)\frac{\ln(2)}{T_{CC}}},$$

resulting in Eq. 3 in Fig. 3B:

$$T^*_{1/2} = \frac{T_{1/2}}{k + (1-k)\frac{T_{1/2}}{T_{cc}}}$$

This model suggests that when intra-cellular degradation decreases the result is a global increase in half-lives but stable proteins are expected to be the least affected. This is illustrated in Figure S8, where predicted lines are generated by fixing the measured cell cycle length, T_{cc}, to 22.5 and applying different k's (reflecting different levels of degradation shutdown). It can be seen that for any value of k, the present model is insufficient to recapitulate the measured half-life increase.

5.5 YFP insertion and the N-terminal rule

One important determinant of protein in-vivo half-life is the amino-acid at its N-terminus (the N-terminal rule) (*26-27*). The YFP tagged proteins in the present library, were inserted as an artificial internal exon (mainly exons 2-5) (*7, 11*). Hence, the YFP tags do not abolish the N-terminal amino-acids and are less likely to interfere with the degradation signals than N-terminal fusions to fluorescent proteins.

5.6 Temporal resolution of bleach-chase

When performing bleach-chase using time-lapse microscopy one can achieve high temporal resolution (order of minutes) for hours and even days. The temporal resolution of bleach-chase is limited by the rate of the fluorescent tag folding and maturation, which ranges between a few minutes and two hours, depending on the type of fluorophore and environmental condition (*28-30*). Proteins that are constitutively degraded at a rate faster than fluorophore maturation time would therefore not be observable using the present assay.

5.7 Additional applications of bleach-chase

The present approach can be used to study protein degradation in different cellular compartments (e.g. nucleus versus cytoplasm) because bleach-chase allows a microscopy-based assay of protein removal. Additionally, bleach-chase facilitates measurements of degradation rates as a function of cell-cycle stage, without the need for chemical or physical synchronization. This can be achieved by applying bleach-chase to a population of unsynchronized cells, followed by in-silico synchronization (*7, 11*). Finally, one can use bleach-chase to retrieve *protein production rates* by using the measured removal rate and protein levels and applying Eq. 2 in Box S1.

SOM References

1. J. Monod, A. M. Pappenheimer, Jr., G. Cohen-Bazire, *Biochim Biophys Acta* **9**, 648 (Dec, 1952).
2. U. Alon, *An introduction to systems biology : design principles of biological circuits*. Chapman & Hall/CRC mathematical and computational biology series (Chapman & Hall/CRC, Boca Raton, FL, 2007), pp. xvi, 301 p., 4 p. of plates.
3. J. W. Jarvik, S. A. Adler, C. A. Telmer, V. Subramaniam, A. J. Lopez, *Biotechniques* **20**, 896 (May, 1996).
4. J. W. Jarvik, C. A. Telmer, *Annu Rev Genet* **32**, 601 (1998).
5. J. W. Jarvik *et al.*, *Biotechniques* **33**, 852 (Oct, 2002).
6. A. Sigal *et al.*, *Nat Protoc* **2**, 1515 (2007).
7. A. A. Cohen *et al.*, *Science* **322**, 1511 (Dec 5, 2008).
8. X. Morin, R. Daneman, M. Zavortink, W. Chia, *Proc Natl Acad Sci U S A* **98**, 15050 (Dec 18, 2001).
9. P. J. Clyne, J. S. Brotman, S. T. Sweeney, G. Davis, *Genetics* **165**, 1433 (Nov, 2003).
10. W. K. Huh *et al.*, *Nature* **425**, 686 (Oct 16, 2003).
11. A. Sigal *et al.*, *Nat Methods* **3**, 525 (Jul, 2006).
12. D. Axelrod, D. E. Koppel, J. Schlessinger, E. Elson, W. W. Webb, *Biophys J* **16**, 1055 (Sep, 1976).
13. J. Lippincott-Schwartz, N. Altan-Bonnet, G. H. Patterson, *Nat Cell Biol* **Suppl**, S7 (Sep, 2003).
14. R. Ando, H. Hama, M. Yamamoto-Hino, H. Mizuno, A. Miyawaki, *Proc Natl Acad Sci U S A* **99**, 12651 (Oct 1, 2002).
15. G. H. Patterson, J. Lippincott-Schwartz, *Science* **297**, 1873 (Sep 13, 2002).
16. M. Buszczak *et al.*, *Genetics* **175**, 1505 (Mar, 2007).
17. E. Eden, D. Lipson, S. Yogev, Z. Yakhini, *PLoS Comput Biol* **3**, e39 (Mar 23, 2007).
18. E. Eden, R. Navon, I. Steinfeld, D. Lipson, Z. Yakhini, *BMC Bioinformatics* **10**, 48 (2009).
19. A. Tzur, R. Kafri, V. S. LeBleu, G. Lahav, M. W. Kirschner, *Science* **325**, 167 (Jul 10, 2009).
20. R. Y. Hampton, A. Koning, R. Wright, J. Rine, *Proc Natl Acad Sci U S A* **93**, 828 (Jan 23, 1996).
21. X. Li *et al.*, *J Biol Chem* **274**, 21244 (Jul 23, 1999).
22. L. Zhang *et al.*, *Biotechniques* **42**, 446 (Apr, 2007).
23. S. Bellanger, C. Demeret, S. Goyat, F. Thierry, *J Virol* **75**, 7244 (Aug, 2001).
24. S. Ghaemmaghami *et al.*, *Nature* **425**, 737 (Oct 16, 2003).
25. A. Belle, A. Tanay, L. Bitincka, R. Shamir, E. K. O'Shea, *Proc Natl Acad Sci U S A* **103**, 13004 (Aug 29, 2006).
26. A. Ciechanover, A. L. Schwartz, *Trends Biochem Sci* **14**, 483 (Dec, 1989).
27. A. Varshavsky, *Genes Cells* **2**, 13 (Jan, 1997).
28. J. A. Megerle, G. Fritz, U. Gerland, K. Jung, J. O. Radler, *Biophys J* **95**, 2103 (Aug, 2008).
29. R. Y. Tsien, *Annu Rev Biochem* **67**, 509 (1998).
30. T. Nagai *et al.*, *Nat Biotechnol* **20**, 87 (Jan, 2002).

Figure S1.

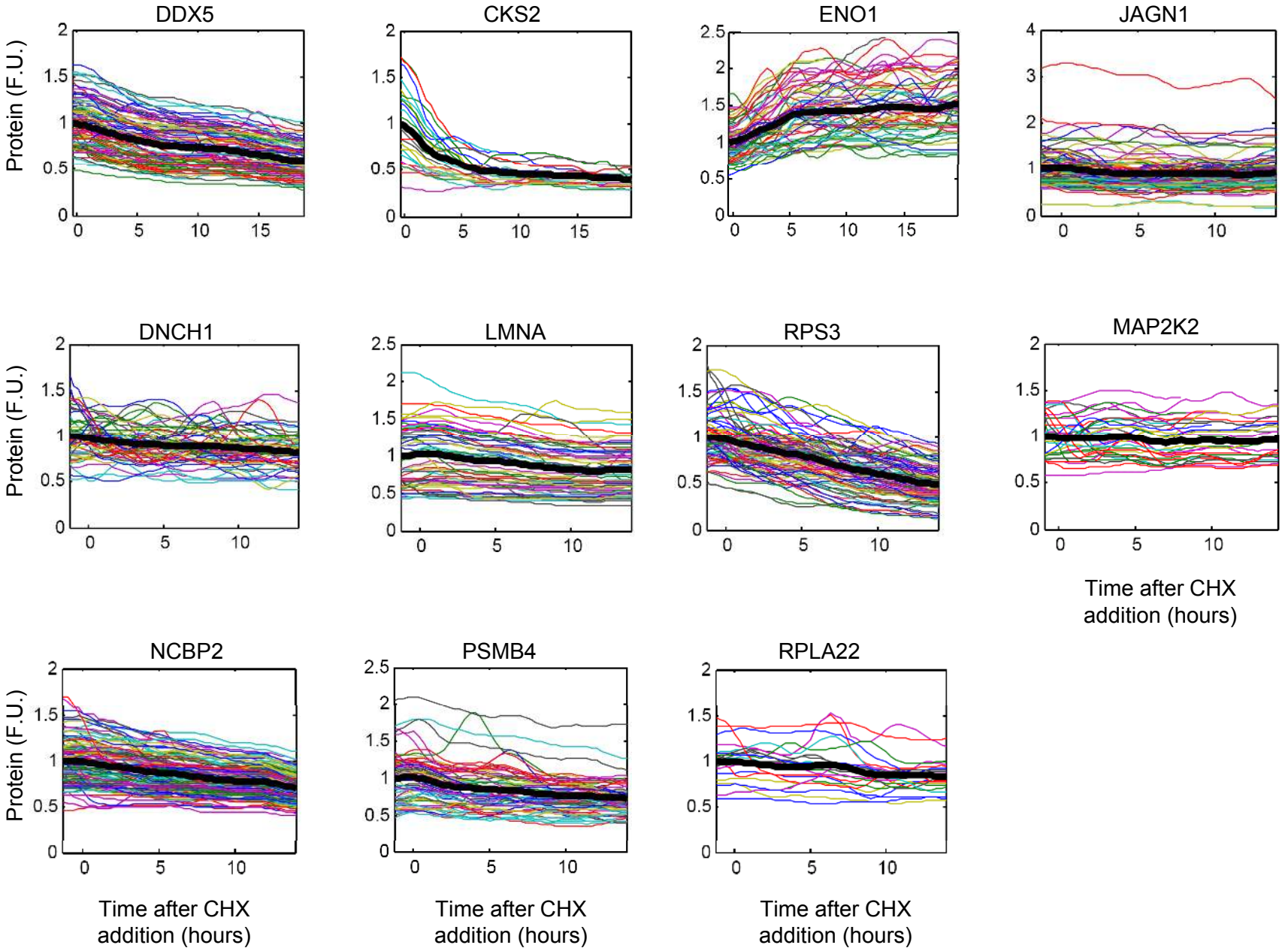
DDX5
CKS2
ENO1
JAGN1
DNCH1
LMNA
RPS3
MAP2K2
NCBP2
PSMB4
RPLA22
Protein (F.U.)
Time after CHX addition (hours)

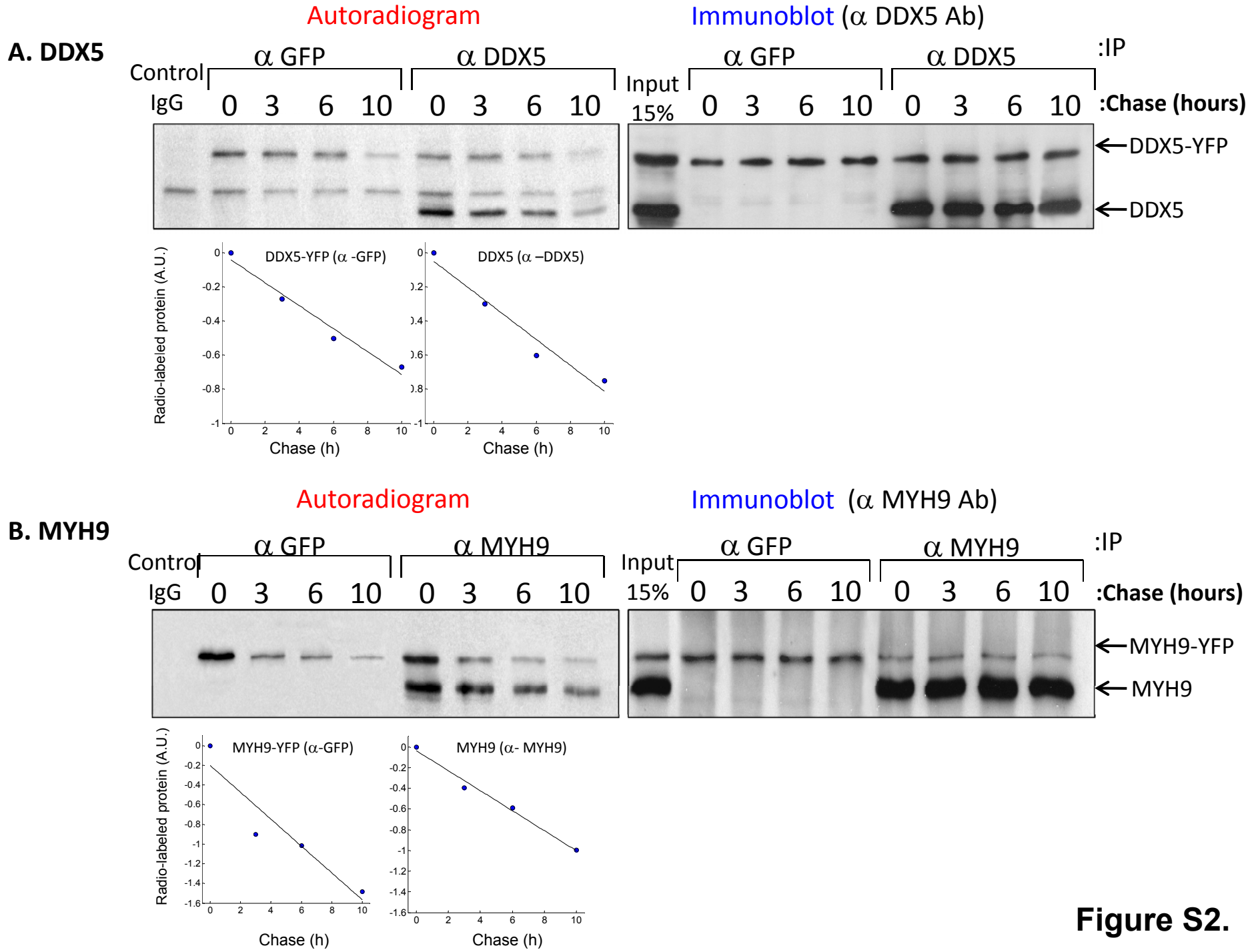
A. DDX5
Autoradiogram
Immunoblot (α DDX5 Ab)
Control IgG
α GFP
α DDX5
:IP
Input 15%
0 3 6 10 0 3 6 10
:Chase (hours)
DDX5-YFP
DDX5
Radio-labeled protein (A.U.)
DDX5-YFP (α -GFP)
DDX5 (α –DDX5)
Chase (h)
B. MYH9
Autoradiogram
Immunoblot (α MYH9 Ab)
Control IgG
α GFP
α MYH9
:IP
Input 15%
0 3 6 10 0 3 6 10
:Chase (hours)
MYH9-YFP
MYH9
Radio-labeled protein (A.U.)
MYH9-YFP (α-GFP)
MYH9 (α- MYH9)
Chase (h)

Figure S2.

Figure S3.

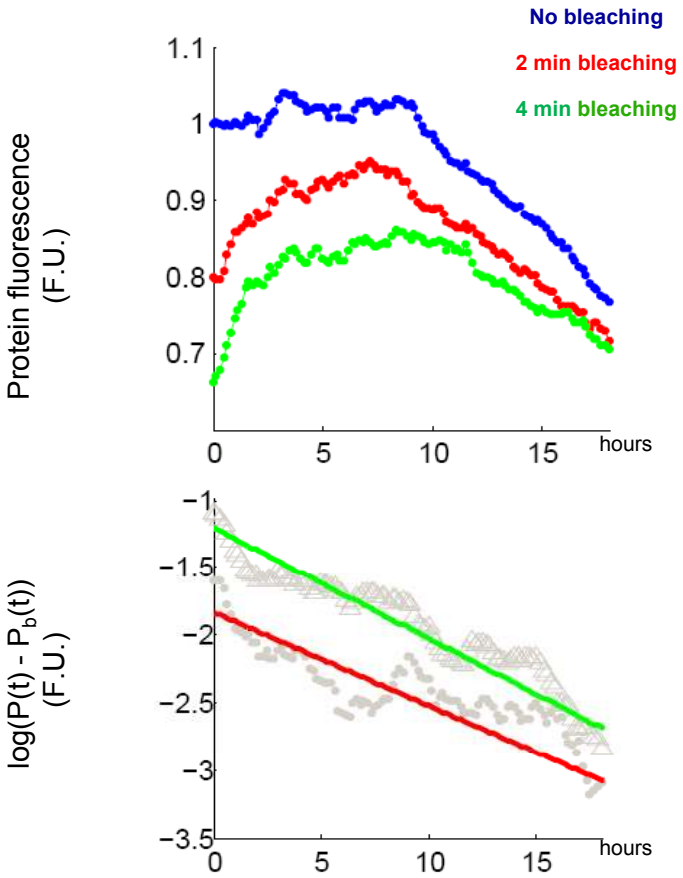
No bleaching
2 min bleaching
4 min bleaching
Protein fluorescence (F.U.)
1.1
1
0.9
0.8
0.7
0
5
10
15
hours
log(P(t) - P_b(t)) (F.U.)
−1
−1.5
−2
−2.5
−3
−3.5
0
5
10
15
hours

Figure S4.

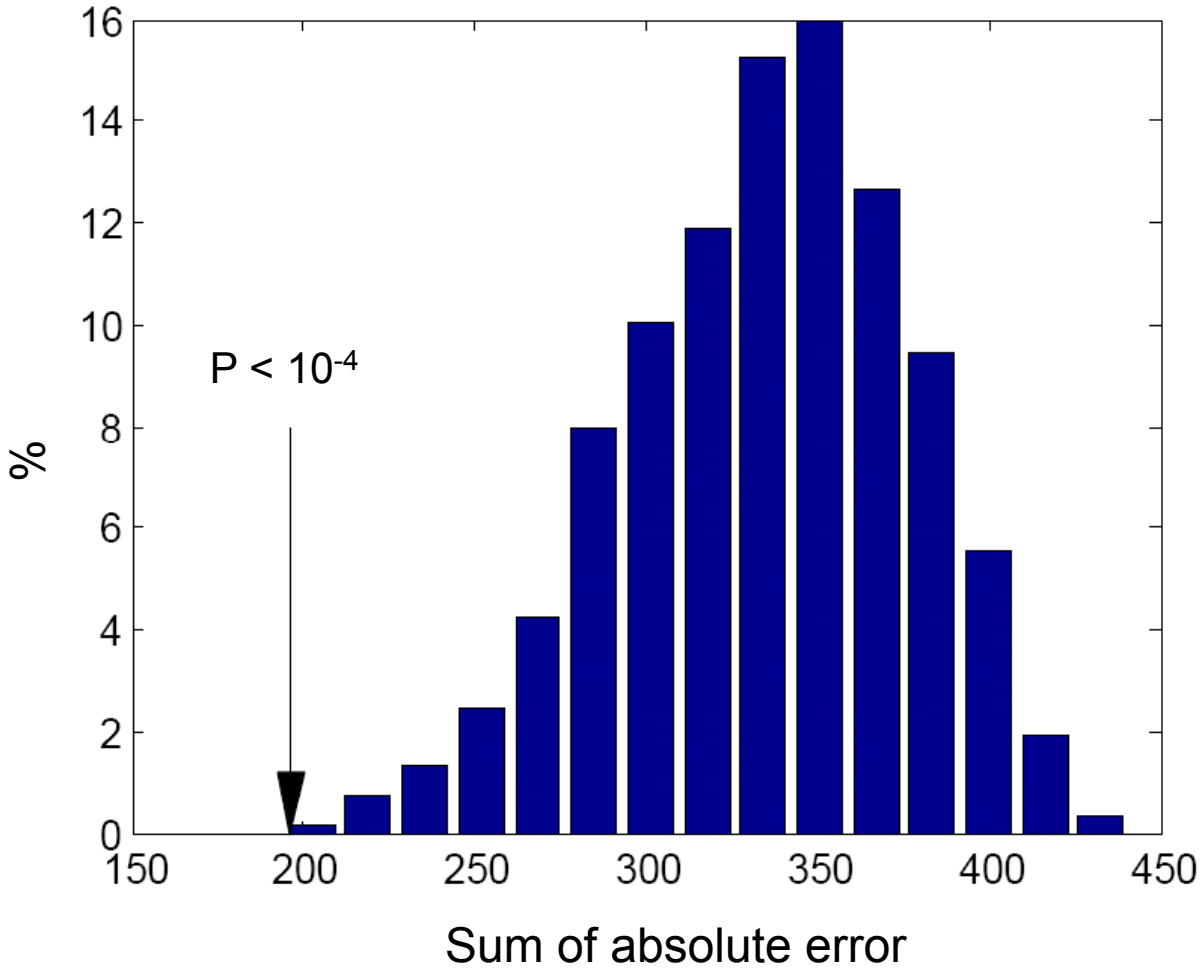
16
14
12
10
8
6
4
2
0
%
P < 10-4
150
200
250
300
350
400
450
Sum of absolute error

Figure S5.

A

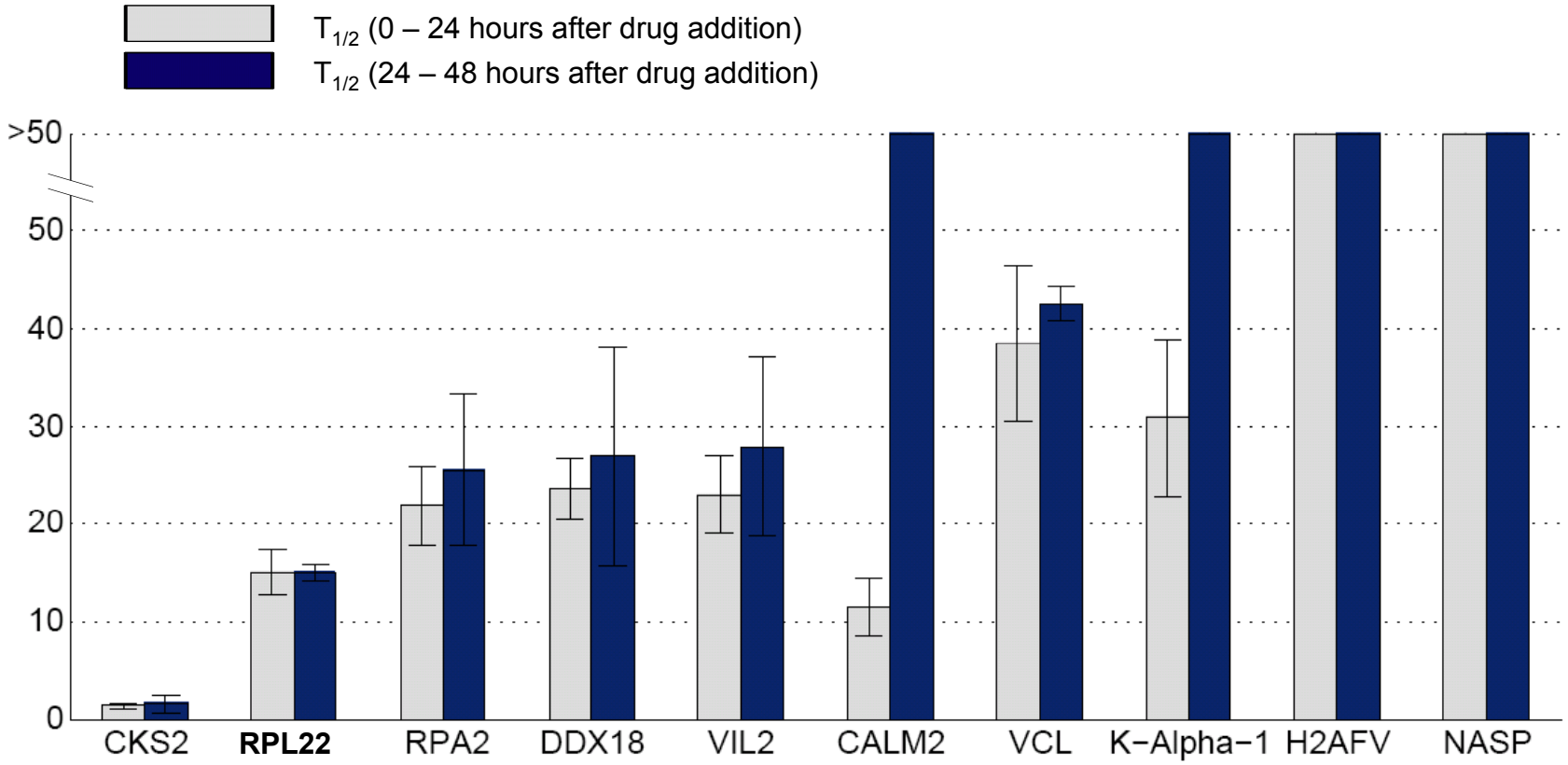
T1/2 (0 – 24 hours after drug addition)
T1/2 (24 – 48 hours after drug addition)
>50
50
40
30
20
10
0
CKS2
RPL22
RPA2
DDX18
VIL2
CALM2
VCL
K−Alpha−1
H2AFV
NASP

B

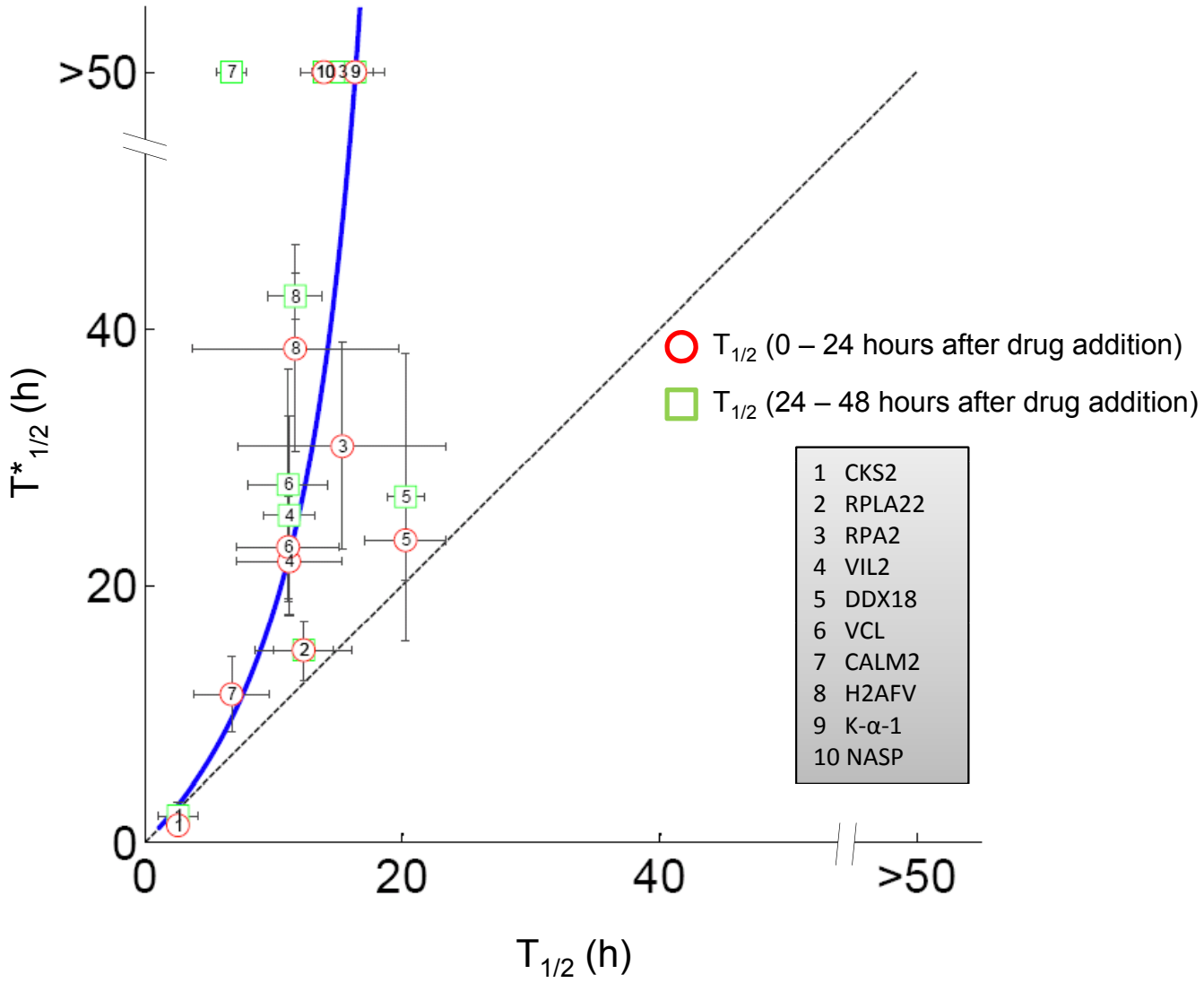
>50
40
20
0
0
20
40
>50
T*1/2 (h)
T1/2 (h)
T1/2 (0 – 24 hours after drug addition)
T1/2 (24 – 48 hours after drug addition)
1 CKS2
2 RPLA22
3 RPA2
4 VIL2
5 DDX18
6 VCL
7 CALM2
8 H2AFV
9 K-α-1
10 NASP

Figure S6.

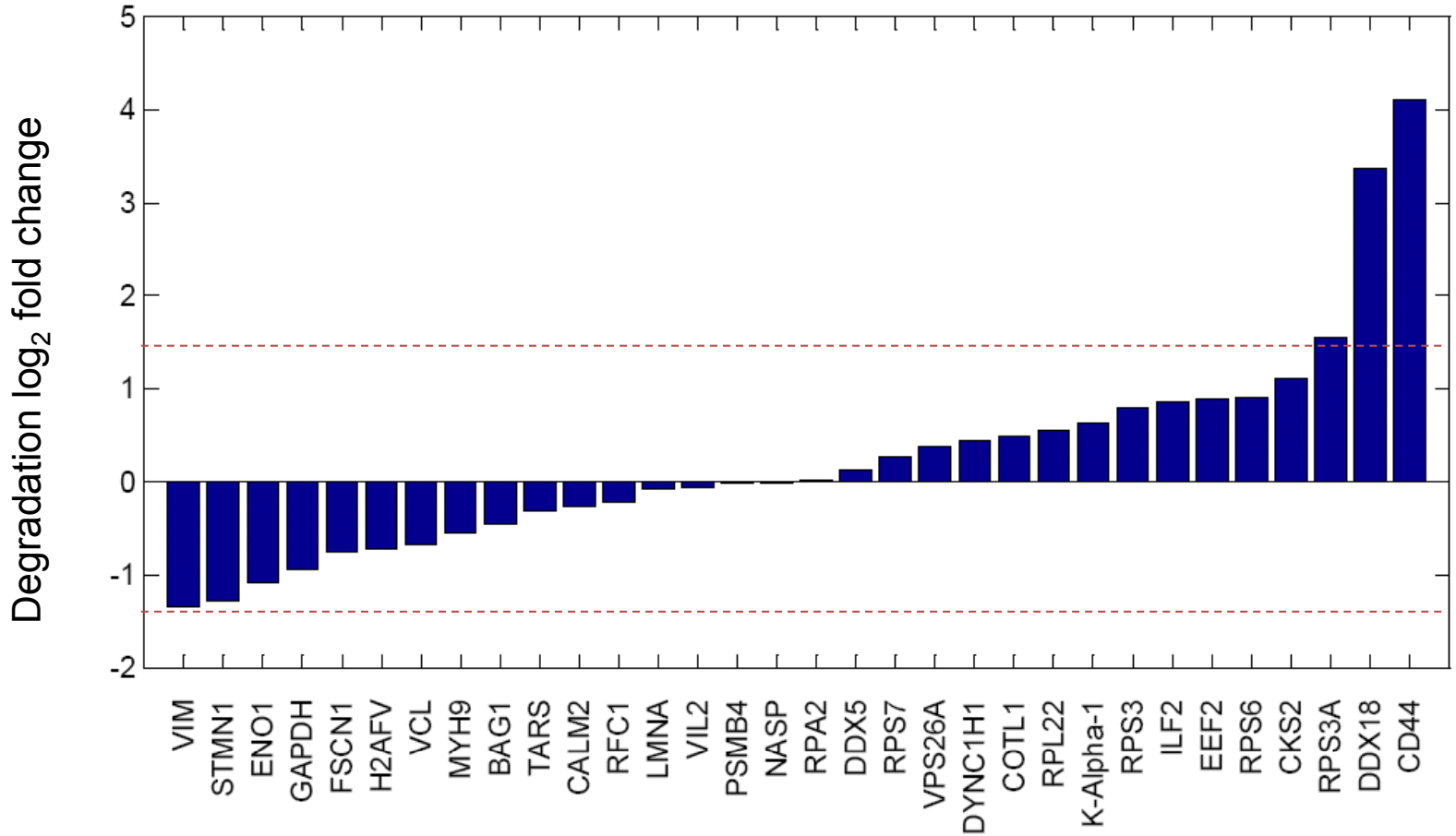
Degradation log2 fold change
5
4
3
2
1
0
-1
-2
VIM
STMN1
ENO1
GAPDH
FSCN1
H2AFV
VCL
MYH9
BAG1
TARS
CALM2
RFC1
LMNA
VIL2
PSMB4
NASP
RPA2
DDX5
RPS7
VPS26A
DYNC1H1
COTL1
RPL22
K-Alpha-1
RPS3
ILF2
EEF2
RPS6
CKS2
RPS3A
DDX18
CD44

Figure S7.

A

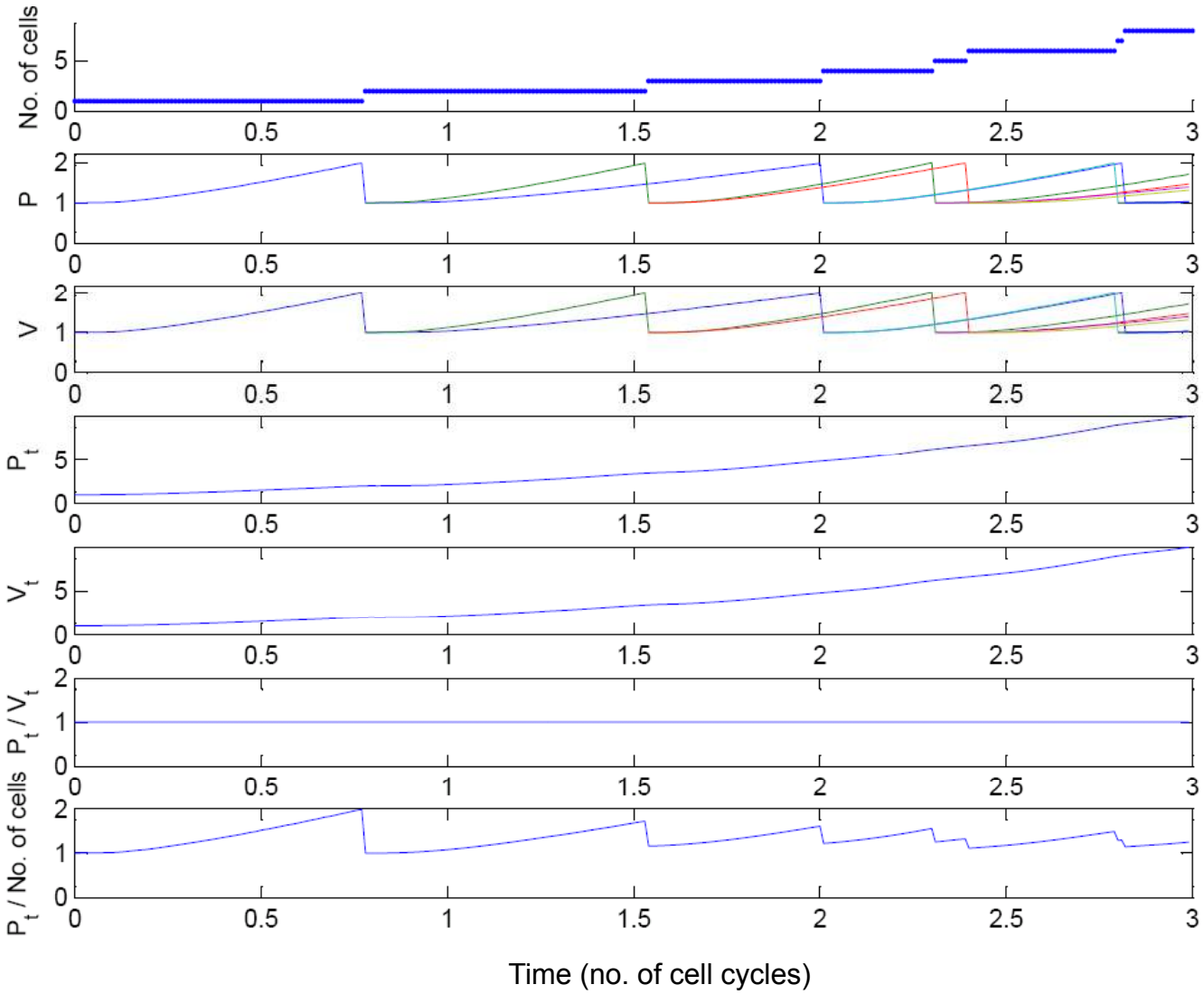

B

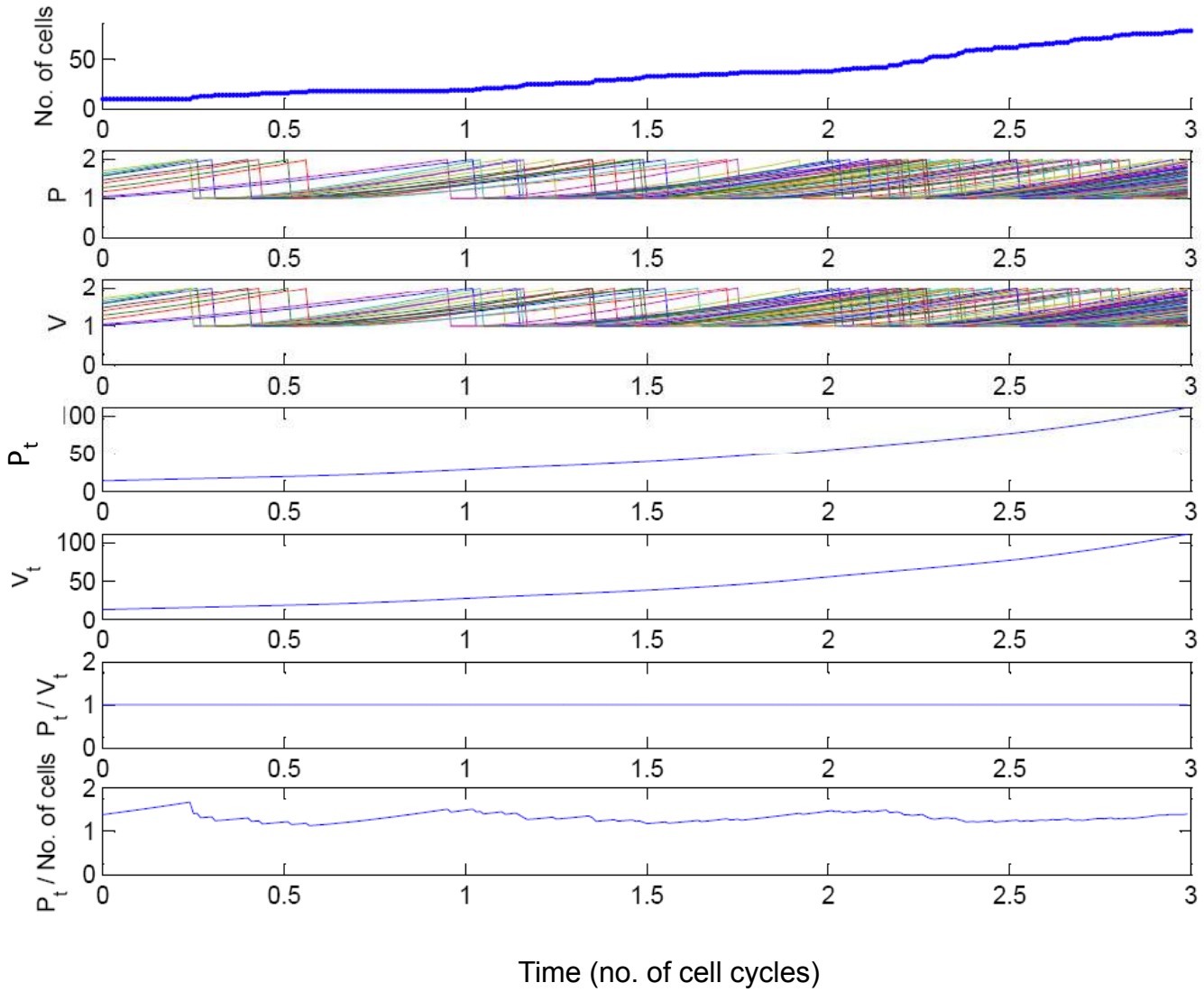

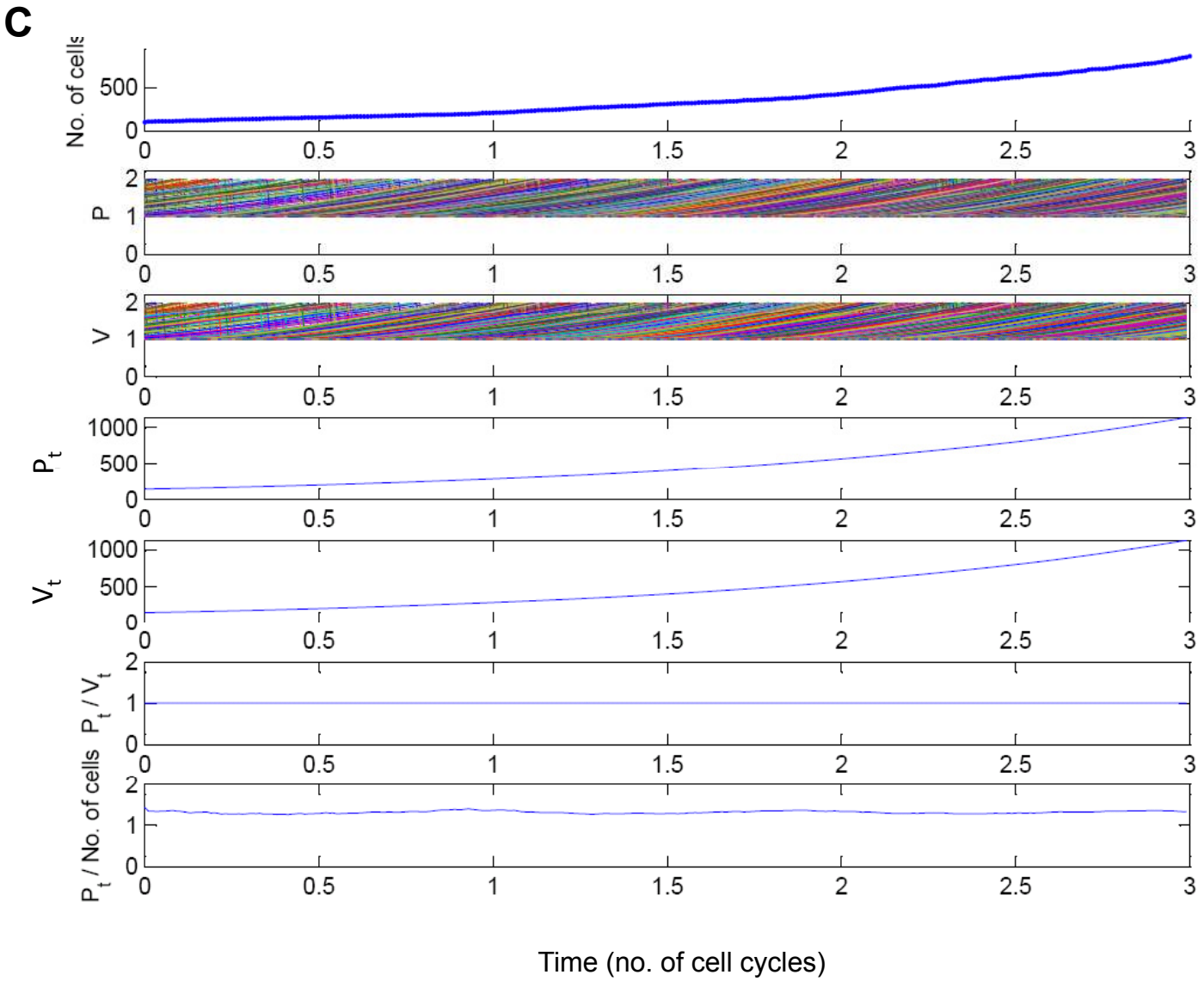
C
No. of cells
500
0
0
0.5
1
1.5
2
2.5
3
P
2
1
0
V
P_t
1000
V_t
P_t / V_t
P_t / No. of cells
Time (no. of cell cycles)

Figure S8.